Research Square

Preprints are preliminary reports that have not undergone peer review.
They should not be considered conclusive, used to inform clinical practice,
or referenced by the media as validated information.

TiO_2 Catalysts Derived from Pyrolysis of Photovoltaic Backsheet PVF Films for Pollutant Degradation

Zhang Xiaojiao
Zhang yang
Yang Jie
Wu Yanlin
Dai Jue
Xu Qin
Guan Jie
guanjie@sspu.edu.cn

Research Article

Keywords: PVF, pyrolysis, TiO_2-based photocatalyst, solid waste recycling, ofloxacin degradation

Posted Date: November 26th, 2026

DOI: https://doi.org/10.21203/rs.3.rs-11758880/v1

License: This work is licensed under a Creative Commons Attribution 4.0 International License.
Read Full License

Additional Declarations: No competing interests reported.

TiO_2 Catalysts Derived from Pyrolysis of Photovoltaic Backsheet PVF Films for Pollutant Degradation

Zhang Xiaojiao[1], Zhang yang[1], YangJie[1], Wu Yanlin[1], Dai Jue[1], XuQin[1,*], Guan Jie[1,*]

([1]School of Resource and Environmental Engineering, Shanghai Polytechnic University, Shanghai 201209)

*Corresponding authors.

E-mail: xuqin@sspu.edu.cn (Xu Qin); guanjie@sspu.edu.cn (Guan Jie).

Abstract: Waste poly(vinyl fluoride) (PVF) photovoltaic backsheets are difficult to degrade and inefficient to recycle. Herein, a one-step pyrolysis strategy is proposed to convert waste PVF films directly into carbon-supported TiO_2 photocatalysts. Thermal analysis was used to determine the optimal preparation conditions, and multiple characterizations were performed to clarify the optical absorption, band structure, elemental distribution, pore architecture and surface chemical states of the products. Photocatalytic tests combined with intermediate identification revealed the degradation pathway of the target pollutant. The results show that rutile TiO_2 is anchored on a carbon skeleton. The pristine pyrolyzed sample exhibits a dense surface and a low specific surface area, and thus limited activity. Acid leaching narrows the direct bandgap from 2.17 to 1.93eV and extends the photoresponse range. Meanwhile, the specific surface area increases by 40% (from 1.1312 to 1.5878 $m^2 \cdot g^{-1}$) and the surface oxygen content rises by 77.7% (from 18% to 32%), introducing abundant hydroxyl groups that promote molecular oxygen adsorption and enrich the active sites, while the Ti^{4+} valence state of the TiO_2 matrix remains essentially unchanged. Under near-neutral conditions, the modified catalyst degrades 87.7% of low-concentration ofloxacin within 90 min, compared with 30.5% for the unmodified sample, without tedious pH adjustment. Decarboxylation, hydroxylation and side-chain cleavage are identified as the main degradation pathways, and a mineralization rate of 16.7% is reached. This work confirms the feasibility of upgrading waste PVF

films into photocatalytic materials and provides a basis for building a green recycling system for PVF solid waste.

Keywords: PVF; pyrolysis; TiO_2-based photocatalyst; solid waste recycling; ofloxacin degradation

1. Introduction

With the continuous advancement of global "dual carbon" goals, the installed capacity of photovoltaic (PV) power generation has grown rapidly, bringing the disposal of end-of-life PV modules to the forefront. It is predicted that by 2050 the global volume of decommissioned PV modules will reach tens of millions of tons[1-2]. As a key encapsulation component, the fluorine-containing PV backsheet has made its harmless disposal and resource recovery a critical link in closing the green loop of the PV industry chain[3]. PV backsheets are typically multilayer composites of a PET substrate, a weather-resistant fluoropolymer film and a polyolefin inner layer. Among various fluoropolymers, PVF and PVDF are the two most widely used weather-resistant films owing to their accessible raw materials and controllable cost[4-5]. PVF, a typical fluoropolymer with the repeating unit —CH_2—CHF—, possesses excellent UV resistance, chemical corrosion resistance, low water absorption and high thermal stability, with a long-term service temperature of -100 to 150°C, and is thus widely used as the outer protective film of PV backsheets. However, this chemical stability also makes retired PVF backsheets difficult to dispose of: incineration releases highly toxic hydrogen fluoride, landfilling leads to long-term environmental persistence, and conventional thermoplastic recycling is inapplicable, causing severe environmental pressure and resource waste[6-7].

The unique thermal decomposition behavior of PVF films offers a feasible route for pyrolytic resource recovery. Domestic studies have largely focused on the pyrolytic recycling of intact end-of-life PV modules: Wang et al. reviewed thermal dissociation technologies and pointed out that the thermal degradation of fluoropolymers tends to generate toxic by-products, which must be strictly controlled[8]. Most domestic reports on PVF pyrolysis concentrate on decomposition kinetics and generally divide the conversion pathway into three steps: end-group elimination, main-chain scission, and the formation of short-chain perfluorocarbons and inorganic fluorides[9].

Recent international studies focus more on fluorine release during backsheet pyrolysis. Agmar et al. confirmed that main-chain scission and HF elimination occur simultaneously at high temperature, accompanied by aromatization and cyclization, ultimately forming fluorinated polycyclic aromatic hydrocarbons[10]. Research from the Fraunhofer Institute indicates that PVF preferentially undergoes dehydrofluorination at 220–350°C to form conjugated polyenes, which are then converted into fluorohydrocarbons, olefins and aromatic fluorides through radical chain reactions; above 450°C the carbon chains cross-link to produce char and perfluorocarbons, while part of the fluorine remains in the solid phase as inorganic fluorides[11]. In addition, Camargo et al. recovered silver and silicon by pyrolyzing PV laminates[12], and Kumagai developed a chemical recycling route based on NaOH hydrolysis of the PET layer to separate the fluorine film[13]. Overall, research specifically targeting PVF backsheet pyrolysis remains limited and deserves further exploration.

Notably, commercial PVF films typically incorporate TiO_2 as a UV-shielding filler. Therefore, besides fluorinated gases (mainly HF), pyrolysis of PVF yields a solid residue composed of TiO_2 and a carbon matrix, which provides an ideal vehicle for the high-value recycling of PVF[14]. Modified TiO_2-based materials have shown good potential in the visible-light-driven purification of antibiotic wastewater[15]; however, pristine TiO_2 photocatalysts generally suffer from severe agglomeration, difficult separation and rapid recombination of photogenerated carriers[16–17]. Directly converting the pyrolysis residue of end-of-life PVF backsheets into photocatalytic materials would therefore address the disposal problem of PVF solid waste while producing functional catalytic materials, achieving the synergistic goal of "treating waste with waste".

Based on the above background, this study adopts a one-step pyrolysis process to convert waste PVF films into TiO_2-based photocatalysts, circumventing the reliance on high-purity precursors. Thermogravimetric analysis determined the optimal pyrolysis temperature, and X-ray diffraction resolved the crystalline phases. Light absorption, morphology, elemental distribution and pore structure were evaluated by UV-Vis-NIR diffuse reflectance spectroscopy, field-emission scanning electron microscopy and automated surface area and porosity analysis, while X-ray photoelectron spectroscopy clarified surface chemical states, elemental valences and

functional groups. Photocatalytic degradation experiments coupled with liquid chromatography-mass spectrometry was conducted to identify intermediates and elucidate the degradation pathway. The photocatalytic activity of the resulting carbon-based composites and the mechanisms underlying the differences among preparation conditions were systematically evaluated, providing new insights for the high-value utilization of waste PVF films.

2. Materials and Methods

2.1 Experimental Materials

PVF films were obtained from decommissioned photovoltaic modules (DuPont TWH15BL3). Ofloxacin (OFL, ≥98%) was purchased from Shanghai Yuanye Bio-Technology Co., Ltd. Nitric acid and calcium hydroxide (analytical grade) were supplied by Shanghai Macklin Biochemical Technology Co., Ltd., and ultrapure water was used throughout.

2.2 Experimental Methods

PVF films were delaminated from decommissioned backsheets, rinsed with deionized water, dried and cut into fragments. The pretreated fragments were pyrolyzed in a tube furnace under N_2 at 300, 330, 360, 390, 420 and 450°C (heating rate 10°C/min, holding time 2h). The experimental procedure is shown in Figure 1. Hydrogen fluoride in the exhaust was absorbed by $Ca(OH)_2$ solution to prevent fluorine pollution. After natural cooling, the black residues were collected and ground. For acid modification, the residues were immersed in 1.0 mol/L HNO_3 at room temperature for 12h, then heated to 70°C and held for 3h to selectively remove excess carbon, followed by centrifugation, washing with ultrapure water to neutrality and vacuum drying at 60°C for 12h to obtain the acid-leached titanium-based photocatalytic materials.

Ofloxacin was selected as the target pollutant, since its concentration in pharmaceutical wastewater and contaminated surface water typically ranges from 0.5 to 5mg/L. The initial OFL concentration was set at 0.72mg/L (2μM) with a catalyst dosage of 0.2g/L. Typically, 5mg of the ground sample was dispersed in 25mL of the pollutant solution in a photocatalytic reaction chamber, stirred in the dark for 30 min to establish adsorption–desorption equilibrium while assessing the adsorption capacity, and then irradiated by a 350W xenon lamp equipped with a 290nm cutoff filter to

simulate natural sunlight. Aliquots were withdrawn at 15, 30, 60 and 90 min and analyzed by HPLC with methanol/0.1% phosphoric acid (4:6, v/v) as the mobile phase at 1.00mL/min, a column temperature of 35 °C and a detection wavelength of 294nm.

Thermal analysis was performed on an STA449F3 simultaneous thermal analyzer under N_2 from 25 to 600°C at 0.1°C/min. Crystal structures were characterized on a Bruker D8 Advance diffractometer over 2θ = 10°–80°. UV-Vis diffuse reflectance spectra (200–600nm) were recorded on a UV-3600i Plus spectrophotometer with an integrating sphere. Morphology was observed by S-4800 SEM at 10kV and 700–1000×. Pore structure was measured on a Belsorp-max analyzer using Ar as the adsorbate. XPS survey and high-resolution spectra were acquired with a step size of 0.1eV to analyze surface valence states and functional groups.

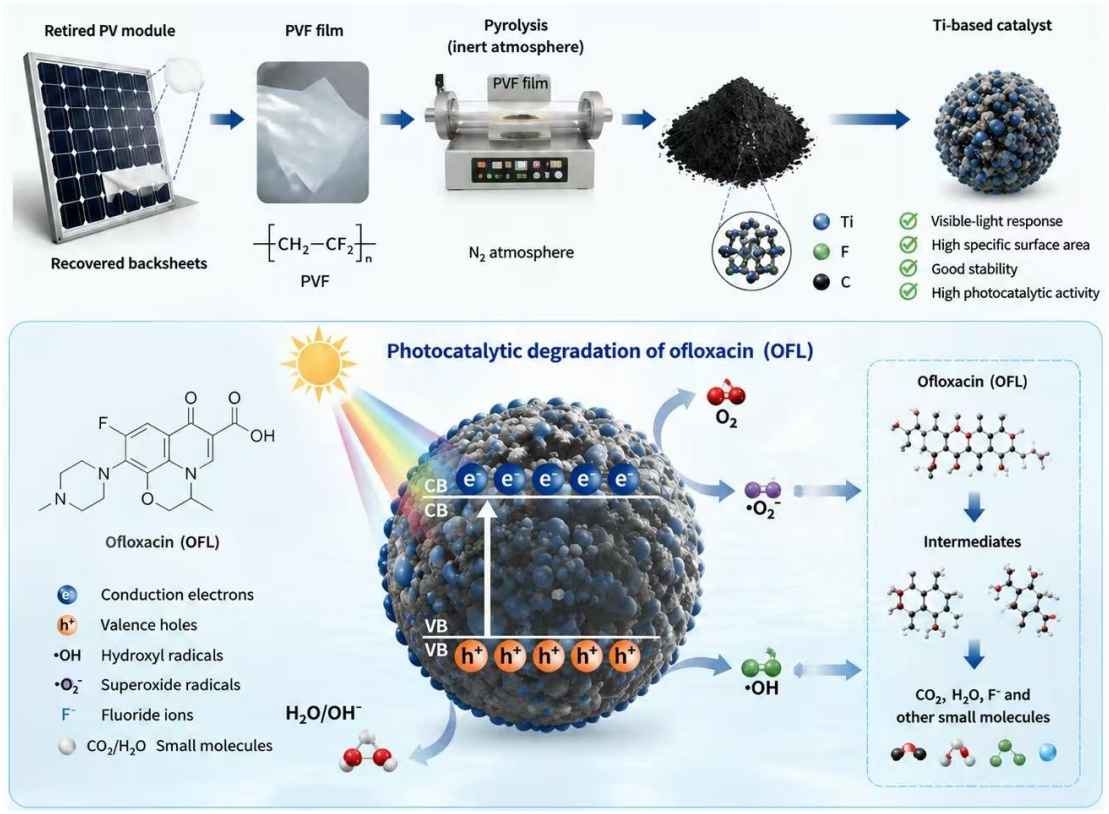

Fig1. Experimental schematic diagram

3. Results and Discussion

3.1 Preparation of Photocatalytic Materials

To clarify the component evolution and thermal stability of PVF during pyrolysis, thermogravimetric analysis was conducted under air from 25 to 600°C (Fig. 2a). Negligible mass loss occurred below 200°C. Above 270°C the mass decreased rapidly, and the main weight loss between 270 and 350°C is attributed to the scission of PVF chains, which generates fluorine and carbon radicals and triggers chain decomposition. A secondary weight loss above 450°C arises from cleavage of the C–C backbone and release of carbon-containing volatiles[18]. Since the target product is TiO_2 from the pyrolysis residue, excessively high temperatures would aggravate the thermal recombination of photogenerated electron–hole pairs and consume active carriers. Accordingly, 300–450°C was selected as the pyrolysis temperature gradient.

Figure 2(b) shows the XRD patterns of the pyrolyzed and acid-leached samples. Both exhibit characteristic peaks at 2θ = 27.4°, 36.1°, 41.2°, 54.4° and 69.0°, corresponding to the (110), (101), (111), (211) and (220) planes of rutile TiO_2 (PDF#79-1640), confirming that TiO_2 remains in the rutile phase after pyrolysis. The peak positions are unchanged after acid leaching, indicating that carbon removal neither destroys the TiO_2 lattice nor alters its crystallinity. The enhanced performance induced by acid leaching is therefore attributed mainly to the removal of surface carbon rather than to a phase change.

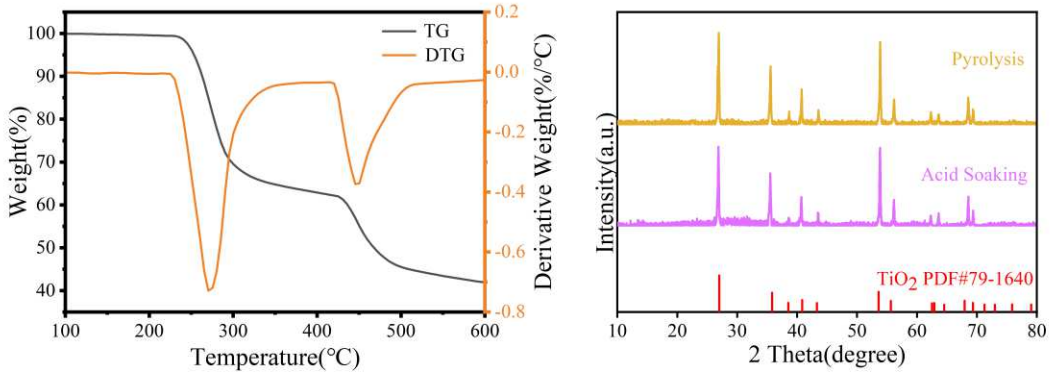

Fig2. (a) Thermogravimetric analysis of PVF; (b) XRD patterns of the material after pyrolysis and acid leaching

3.2 Photocatalytic Performance Evaluation

Photocatalytic degradation of OFL was carried out to evaluate the activity of the catalysts, and the results are presented in Fig. 3(a–f). Figure 3(a) compares samples pyrolyzed at 300–450°C, whose 90 min efficiencies were 30.5%, 27.8%, 27.2%, 26.8%, 25.7% and 27.4%, respectively. The pyrolytic products contain abundant surface carbon, and part of the TiO_2 is encapsulated within the carbon skeleton; high temperatures further accelerate electron–hole recombination and reduce the number of available carriers, so the activity declines overall with increasing pyrolysis temperature. Considering both performance and energy consumption, the 300°C sample was selected for the subsequent single-factor experiments and acid modification. Figure 3(b) shows the effect of initial pollutant concentration: at a fixed dosage of 0.2 g/L, the efficiency decreased from 30.5% to 14.1% as the OFL concentration increased from 2 to 10μM, because the limited number of active sites becomes saturated at higher substrate concentrations.

Acid leaching significantly enhanced the activity (Fig. 3d), and the 90 min efficiency increased from 30.5% to 87.7%. Surface carbon deposits on the pristine sample cover numerous active sites and block contact with pollutants; acid leaching removes this carbon layer and exposes sites such as oxygen vacancies originally wrapped by carbon. Figure 3(e) shows the concentration dependence of the acid-leached sample, whose efficiency dropped from 87.7% to 27.9% when OFL increased from 2 to 10μM, indicating that the system is still limited by active-site saturation at high pollutant loading. The effect of pH is shown in Fig. 3(c) and 3(f): the modified catalyst reached 83.1% at pH 7, superior to pH 3 (30.9%) and pH 9 (27.7%). OFL exhibits different ionization states with pH; at neutral pH it exists mainly as a zwitterion, allowing simultaneous decarboxylation, demethylation and hydroxylation, whereas hydroxylation dominates under acidic conditions and demethylation with piperazine ring oxidation under alkaline conditions, and such single pathways lower the efficiency[19]. Neutral conditions also balance the contributions of various reactive radicals, suppress electron–hole recombination and favor the generation of reactive species, while holes are inhibited in alkaline media and superoxide radicals are less involved in acidic media. The system is therefore suitable for near-neutral water matrices without pH adjustment, showing favorable environmental benignity.

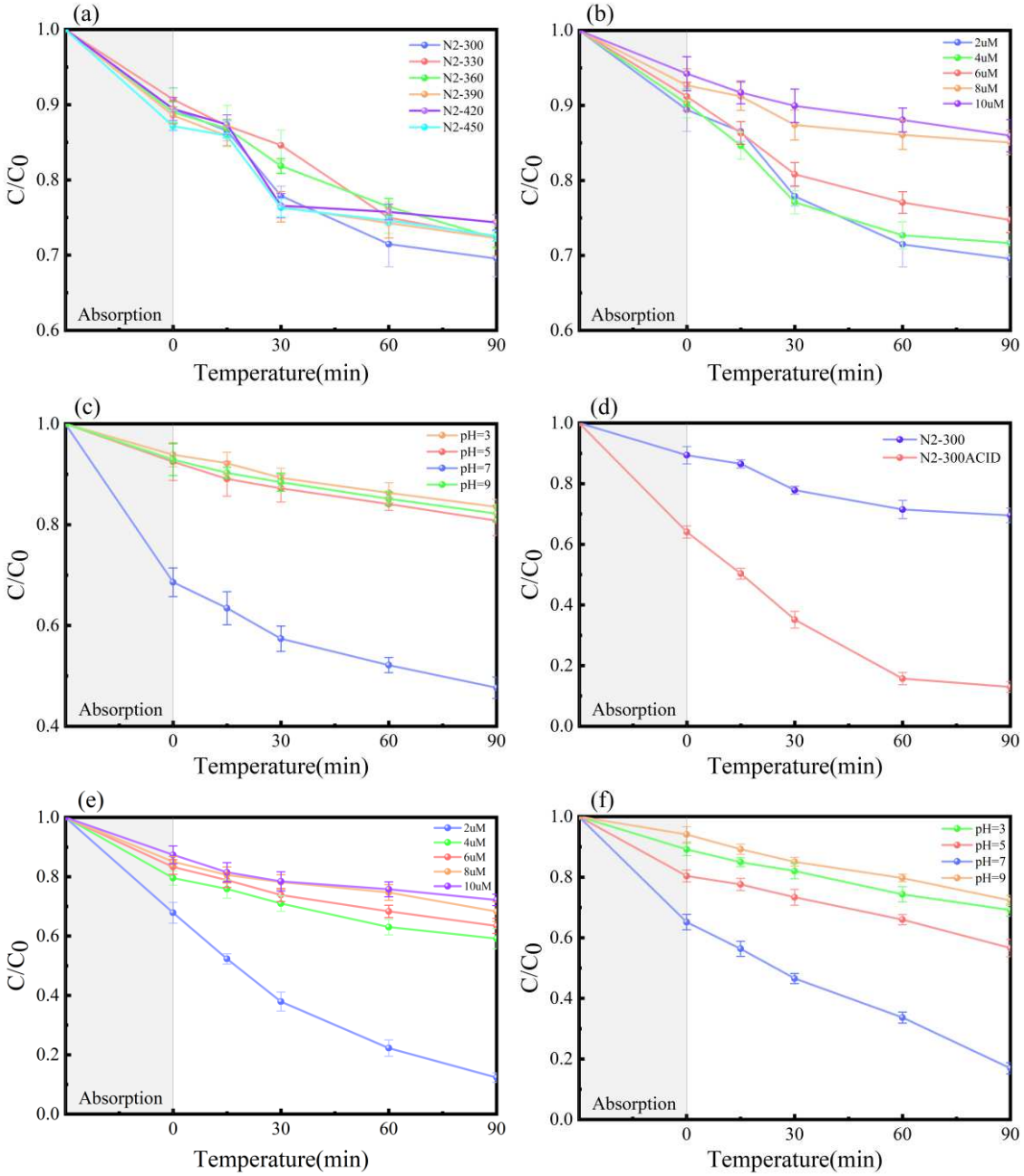

Fig3. Ofloxacin degradation test: (a) effect of pyrolysis temperature; (b) effect of pollutant concentration on the pyrolyzed material; (c) effect of pH on the pyrolyzed material; (d) comparison between the 300 °C pyrolyzed material and the acid-leached material; (e) effect of pollutant concentration on the acid-leached material; (f) effect of pH on the acid-leached material

3.3 Analysis of Differences in Catalytic Performance

As shown in Fig. 4(a), the pyrolyzed sample N300 absorbs at approximately 350 nm, and the absorption edge of the acid-treated sample N300ACID redshifts to longer wavelengths, indicating bandgap narrowing and a reduced energy requirement for

electron transitions[20-21]. Tauc plots (Fig. 4b) confirm that the direct bandgap decreases from 2.17 to 1.93eV after acid leaching. In the 250–450nm range N300ACID exhibits markedly higher absorbance than N300, indicating enhanced light harvesting. Below 250 nm both samples show strong UV absorption ascribed to intrinsic electronic transitions of the skeleton, and its persistence confirms that the main structure survives acid treatment. In the visible region the absorbance of both samples decreases with wavelength, yet N300ACID maintains higher absorption between 400 and 550 nm, demonstrating an extended photoresponse range[22-23]. Acid modification thus regulates the electronic structure, enhances UV-Vis absorption and broadens the photoresponse.

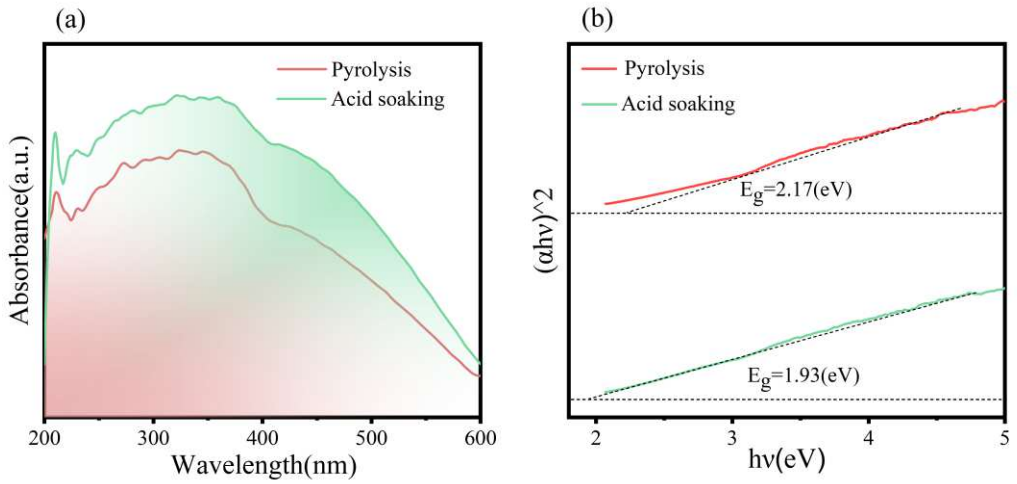

Fig4. (a) UV-Visible absorption spectrum - (b) Direct bandgap energy band of material

Surface morphology was characterized by cold field-emission SEM (Fig. 5). The pyrolyzed material shows a relatively smooth surface (Fig. 5a), implying a small specific surface area that is unfavorable for contact with pollutants and thus limits the activity. After acid leaching (Fig. 5b) the surface is clearly etched and the specific surface area increases substantially, as further verified by N_2 adsorption–desorption (Fig. 6). Both samples exhibit a distinct H3-type hysteresis loop at high relative pressure (P/P_0 = 0.8–1.0), indicating mesopores with slit-shaped channels formed by particle stacking, and the sharp increase in adsorption near $P/P_0 \approx 1.0$ corresponds to macropores from interparticle voids.

The inset pore size distributions show that the pores of both samples are mainly in the mesoporous range (2–50 nm) with a small amount of micropores, and the multiple peaks indicate a heterogeneous hierarchical pore structure. The pore volume

and pore size distribution differ markedly between the two samples, confirming that the modification regulates the pore structure. Such porosity facilitates the diffusion and mass transfer of pollutant molecules. After acid leaching, the specific surface area increased from 1.1312 to 1.5878 $m^2 \cdot g^{-1}$, a gain of 40%, which promotes sufficient contact between the material and pollutants, improves reaction efficiency and thereby enhances the overall photocatalytic performance[24-26].

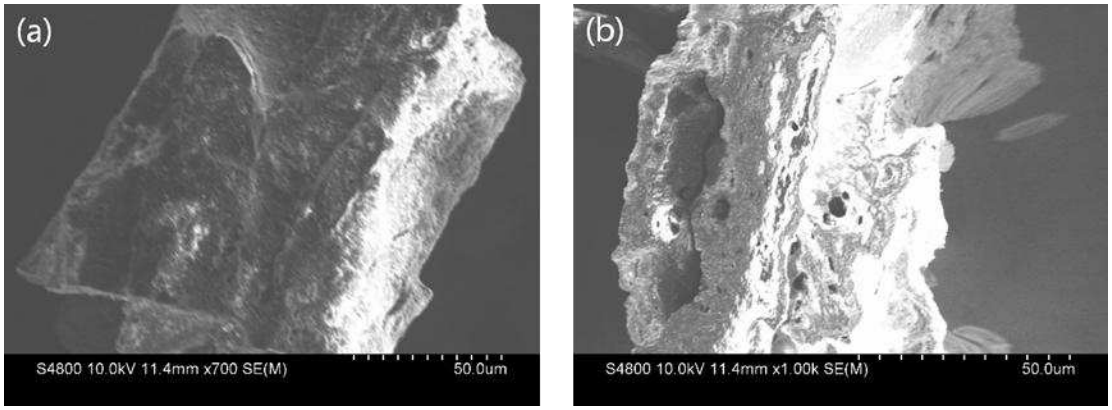

Fig5. SEM image of the material before and after acid leaching

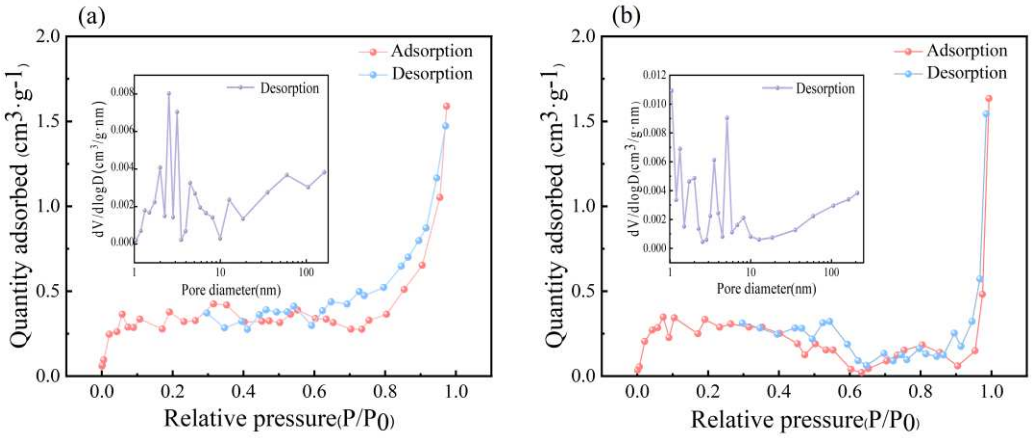

Fig6. (a) Specific surface area and porosity of the material after pyrolysis (b) Specific surface area and porosity of the material after acid leaching

SEM-EDX was used to reveal the spatial elemental distribution, and the results are shown in Figure 7. Five key elements are uniformly distributed throughout the carbon framework. Carbon, the primary framework element, accounts for approximately 67%, while oxygen and titanium show a dispersed, dot-like distribution, suggesting that TiO_2 is the main catalytic component, possibly coexisting with titanium oxyfluoride species.

The abundance of carbon on the surface further suggests that part of the TiO_2 is embedded in the carbon skeleton. Improper encapsulation, such as a carbon layer hindering light absorption by TiO_2 or impeding the separation of photogenerated electron–hole pairs, may account for the inferior activity of the pyrolyzed sample, whereas rational carbon encapsulation can enhance light absorption and electron transfer, and graphitic carbon facilitates carrier separation and suppresses recombination. Comparison with the acid-leached sample (Figure 8) shows that the surface carbon content decreases to 57% while the oxygen content increases from 18% to 32%, a growth rate of 77.7%.

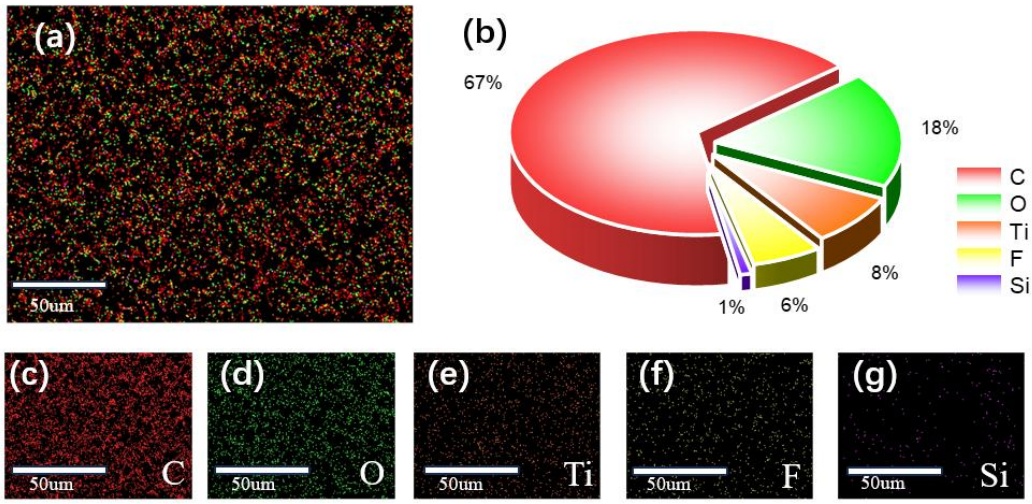

Fig7. Element distribution image and element composition of the material surface after pyrolysis

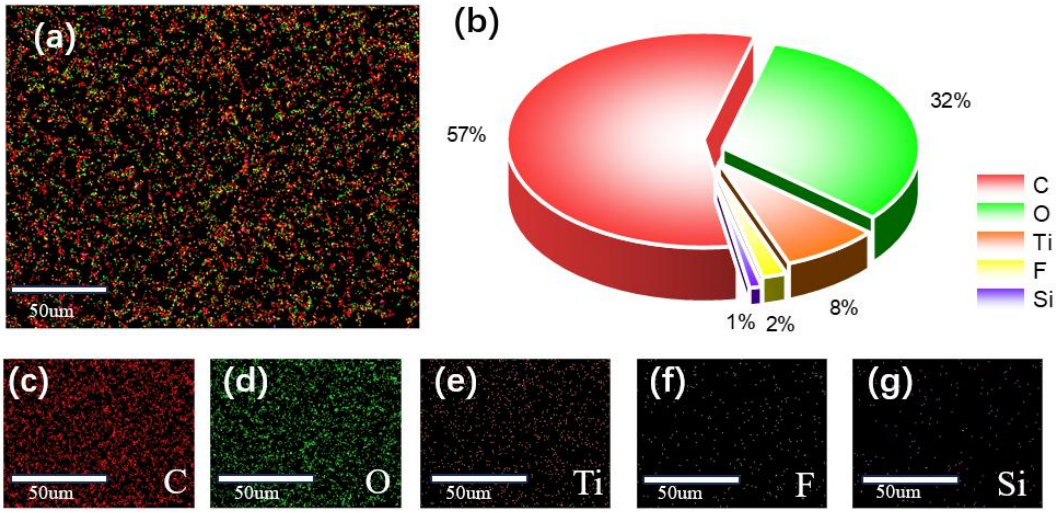

Fig 8. Element distribution image and element composition of the material surface after acid leaching

Figures 9(a) and 9(b) show that the Ti 2p orbital splits into Ti $2p_{3/2}$ and Ti $2p_{1/2}$ peaks. Ti $2p_{3/2}$ is located at 458.4 eV and assigned to Ti^{4+}, while Ti $2p_{1/2}$ appears at 464.0eV (a) and 464.1eV (b). No low-valence titanium signals were detected in either sample, indicating that Ti exists predominantly in the tetravalent state[27], and the negligible peak shift confirms that the chemical state of Ti is essentially unchanged after treatment.

The oxygen signal of the acid-leached sample is markedly stronger than that of the pyrolyzed one. The peak at 529.7eV corresponds to Ti–O lattice oxygen, while the peaks at 531.9–532.1eV arise from surface hydroxyl groups or adsorbed water. Although the relative content of lattice oxygen changes little, the proportion of surface adsorbed oxygen increases, indicating that the modification introduced abundant hydroxyl groups and promoted molecular oxygen adsorption[28-30], while the bulk Ti^{4+} state remained unchanged. This is consistent with the EDS results and suggests that carbon removal exposed oxygen vacancies previously covered by the carbon skeleton, providing additional active sites and thereby enhancing the catalytic performance[31-33].

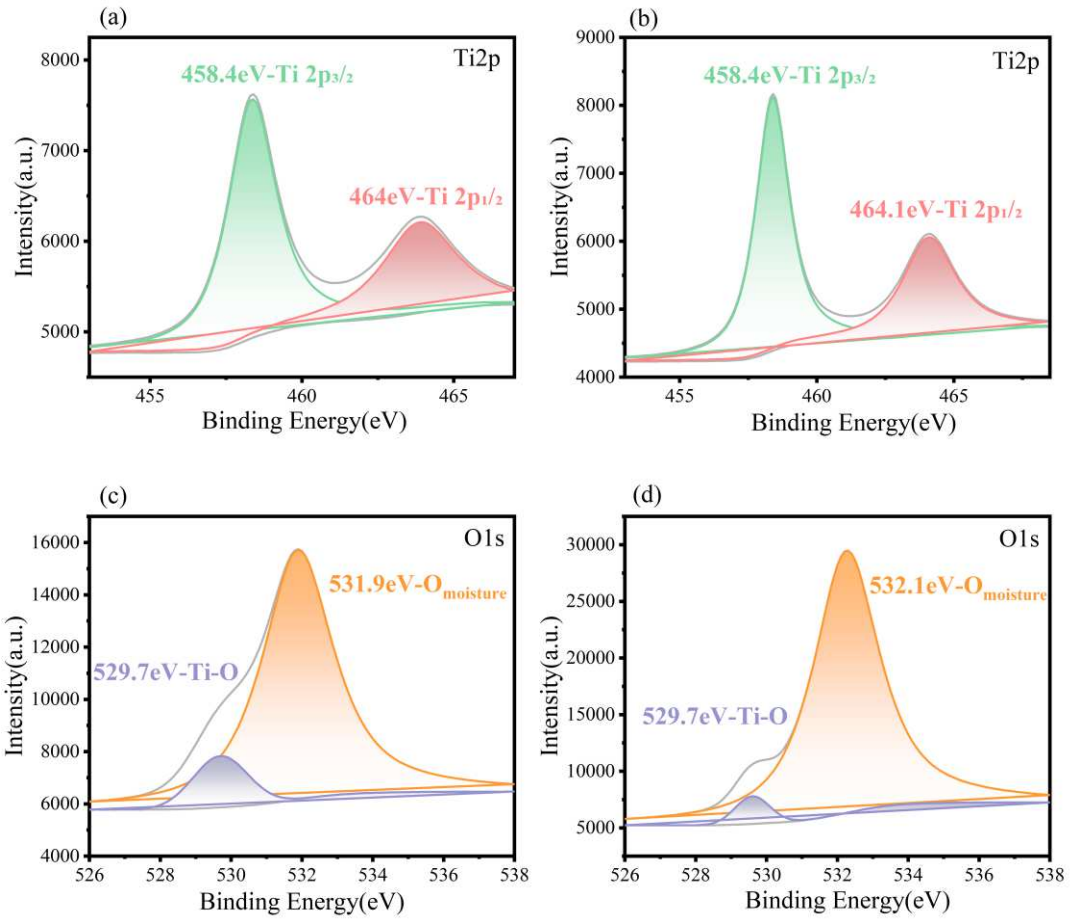

Fig 9. (a) Ti XPS spectra of the material after pyrolysis; (b) Ti XPS spectra of the material after acid leaching; (c) O XPS spectra of the material after pyrolysis; (d) O XPS spectra of the material after acid leaching

3.4 Pollutant Degradation Pathway Analysis

As shown in Fig. 10, the degradation of ofloxacin proceeds through three parallel pathways. In pathway I, the product at m/z=318 corresponds to the decarboxylated intermediate, a classic route for ofloxacin and the dominant one here[34], which is driven mainly by oxidative attack of reactive species such as photogenerated holes (h^+) and hydroxyl radicals[35]; the enriched surface hydroxyl groups and enhanced oxygen adsorption revealed by XPS favor this route. In pathway II, hydroxyl radicals attack the 4-keto position, producing hydroxylated or ketonized intermediates that undergo further cleavage. In pathway III, the product at m/z=360 is an initial oxidation product formed by the loss of two hydrogen atoms from the parent molecule, and m/z =346 arises from side-chain cleavage induced by β-oxidation or radical attack[36-37].

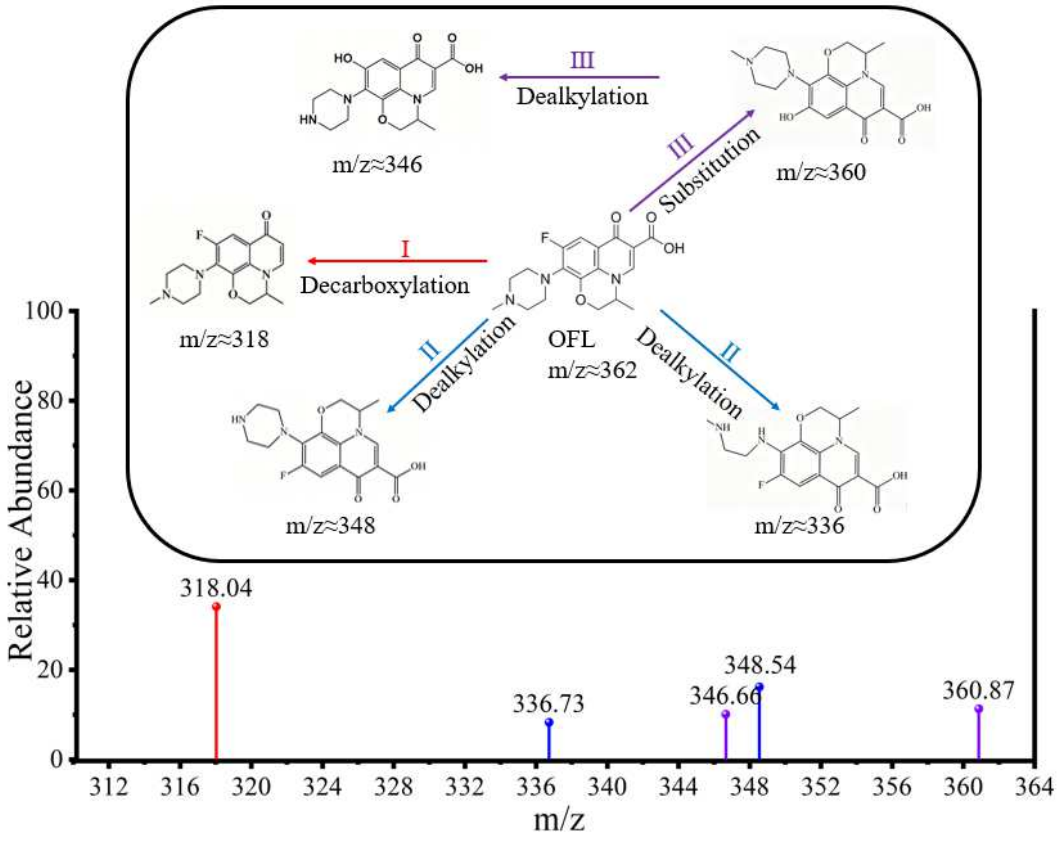

Fig. 10 Degradation pathway diagram of ofloxacin

3.5 Environmental Impact Assessment

Since PVF is a fluoropolymer, improper disposal may cause severe environmental consequences, and incineration and oxygen-free pyrolysis are the common industrial options[38]. Modeling was performed with GaBi software, and 10 impact categories were selected based on previous studies[39]. Figure 11 compares the midpoint environmental impacts of the two routes. Global warming potential (GWP) is the most significant burden of pyrolysis, which also contributes to ozone depletion and photochemical ozone formation; however, pyrolysis consumes far fewer fossil resources and thus has a clear advantage in fossil resource depletion. The differences in acidification and eutrophication potentials are minor. Incineration causes markedly higher human, freshwater and marine ecotoxicity, whereas pyrolysis shows a substantial advantage. In summary, pyrolysis offers lower human and aquatic ecotoxicity, and although its GWP is slightly higher than that of incineration, the values are close; pyrolysis was therefore adopted as the disposal route in this study.

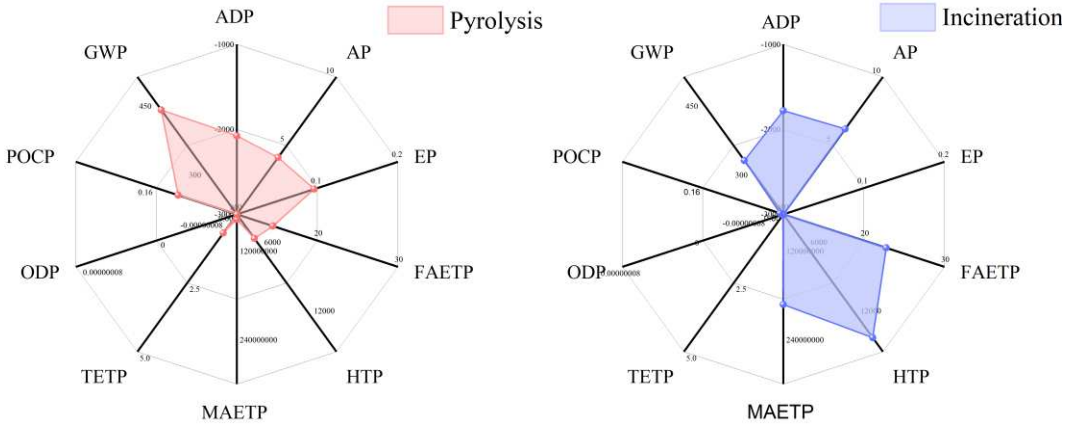

Fig 11. Impact of two PVF treatment methods, pyrolysis and incineration, on the environment

4 Conclusion

In this work, TiO_2 photocatalysts were fabricated from waste PVF films of retired photovoltaic backsheets by one-step pyrolysis combined with acid-leaching modification, and their phase, microstructure, optical properties and photocatalytic degradation of ofloxacin were systematically investigated. One-step pyrolysis directly yields rutile TiO_2 supported on a carbon matrix, with 300°C identified by thermogravimetric analysis as the optimal temperature. The TiO_2 in the pyrolyzed product is encapsulated by carbon, resulting in a low specific surface area and

restricted activity. Acid leaching greatly improves the activity without destroying the rutile phase, and the Ti^{4+} valence state remains essentially unchanged. Acid etching increases the specific surface area by 40%, raises the surface oxygen content by 77.7% and introduces abundant hydroxyl groups, while narrowing the direct bandgap from 2.17 to 1.93eV, which broadens the photoresponse range and provides more active sites. The modified catalyst degrades 87.7% of low-concentration ofloxacin within 90 min under near-neutral conditions without pH adjustment. LC-MS analysis indicates that decarboxylation, hydroxylation and side-chain cleavage dominate the degradation pathways, and TOC measurements give a mineralization rate of 16.7%. Life cycle assessment shows that pyrolysis substantially reduces human and aquatic ecotoxicity compared with incineration, making it a preferable route for waste PVF films. This study realizes the upcycling of waste PVF backsheets and eliminates the reliance on high-purity precursors, providing an experimental foundation for the recovery of fluorine-containing photovoltaic solid waste.

References

[1] Zhang J W, Wang H D, Zhang S G, et al. Research on new process for separation of silicon wafers and glass from decommissioned photovoltaic modules[J]. Physicochemical Problems of Mineral Processing, 2022, 58(6).

[2] Ardente F, Latunussa C E L, Blengini G A. Resource efficient recovery of critical and precious metals from waste silicon PV panel recycling[J]. Waste Management, 2019, 91.

[3] Ahmed S. Solar PV End-of-Life Waste Recycling: An Assessment of Mechanical Recycling Methods and Proposed Hybrid Laser and High Voltage Pulse Crushing Method[J]. Resources, 2024, 13.

[4] Guy Beaucarne, Gabriele Eder, Emmanuel Jadot, et al. Repair and preventive maintenance of photovoltaic modules with degrading backsheets using flowable silicone sealant[J]. Progress in photovoltaics,2022,30(8):1045-1053.

[5] Zhang J W, Deng W, Ye Z, et al. Aging phenomena of backsheet materials of photovoltaic systems for future zero-carbon energy and the improvement pathway[J]. Journal of Materials Science & Technology, 2023.12.063.

[6] Lohmann R, Cousins I T, Dewitt J C, et al. Are Fluoropolymers Really of Low Concern for Human and Environmental Health and Separate from Other PFAS[J]. Environmental Science & Technology: ES&T, 2020(20):54.

[7] Krolikowski M, Ach P. Experimental Investigations for Recycling and Characterisation of EVA, PVF and PET Polymers from Waste Photovoltaic Modules[J]. ECS Meeting Abstracts,

2023-02(49):3269-3269.
[8] Wang M, Zhong H, Bai B, et al. A review on dissociation and resource utilization of decommissioned crystalline silicon photovoltaic modules[J]. Meitan Xuebao, 2024, 49(10):4188-4202.
[9] Shao H，Cheng Z K，Cao R Z，et al. A review on pyrolysis and defluorination mechanisms of perfluoroalkyl substances（PFASs）[J] Environmental Engineering，2025，43（8）：49-59.
[10] Agmar José de Jesus Silva, Costa M F D, Nascimento C R, et al. Kinetics of thermal degradation and lifetime study of poly (PVDF) subjected to bioethanol fuel accelerated aging[J]. Heliyon, 2020, 6(7):1-12.
[11] Danz P, Aryan V, Mhle E, et al. Experimental Study on Fluorine Release from Photovoltaic Backsheet Materials Containing PVF and PVDF during Pyrolysis and Incineration in a Technical Lab-Scale Reactor at Various Temperatures[J]. Toxics, 2019, 7(3).
[12] Camargo P, Domingues A D S, Palomero J P G, et al. Photovoltaic module recycling: thermal treatment to degrade polymers and concentrate valuable metals [J]. Detritus 2021,15119
[13] Kumagai S, Hirahashi S, Grause G, et al. Alkaline hydrolysis of PVC-coated PET fibers for simultaneous recycling of PET and PVC[J]. Journal of Material Cycles & Waste Management, 2018,20(1):439-449.
[14] Liu J, Yao H, Zhang X, et al. Electrospun PVDF/PVP Fibrous Membrane with Photocatalytic and Superhydrophilic Properties[J]. Langmuir, 2024, 40(44):23169-23177.
[15] Sharma M, Yadav A, Mandal M K, et al. TiO2 based photocatalysis: a valuable approach for the removal of pharmaceuticals from aquatic environment[J]. International Journal of Environmental Science and Technology, 2023, 20(4):4569-4584.
[16] Deligiannakis Y, Bletsa E, Mouzourakis E, et al. Carbon-Coated TiO2 Nanoparticles for Noble-Metal-Free Photocatalytic H2 Production from H2O[J]. ACS Applied Nano Materials, 2024, 7(10):13.
[17] Cheng Z, Li C, Zhang X. Bo C. Sun Y. Piao L. Precise design of TiO2 photocatalyst for efficient photocatalytic H2 production from seawater splitting[J]. International journal of hydrogen energy, 2024, 55(Feb.):542-549.
[18] Jiang Y, Zhou W, Jiang M, et al. Flame retardant study of formalized polyvinyl alcohol fiber coated with melamine formaldehyde resins and the synergistic effect of copper ions[J]. Polymer Degradation and Stability, 2017, 144(oct.):331-343.
[19] Chen X, Yao J, Xia B, et al. Influence of pH and DO on the ofloxacin degradation in water by UVA-LED/ TiO_2 nanotube arrays photocatalytic fuel cell: mechanism, ROSs contribution and power generation[J]. Journal of Hazardous Materials, 2020, 383(Feb.5):121220.1-121220.11.

[20] Zhong W, Fu W, Sun, S, et al. Characterization of TiO2 and an as-prepared TiO2/SiO2 composite and their photocatalytic performance for the reduction of low-concentration N-NO3- in water[J]. Environmental Science and Pollution Research,2022,29(27):40585-40598.

[21] Chen L, Gao Z, Li Q, et al. A review: Comprehensive investigation on bandgap engineering under high pressure utilizing microscopic UV–Vis absorption spectroscopy[J].APL Materials, 2024, 12(3):030602-030602-21.

[22] Wannakan K, Khansamrit K, Senasu T, et al. Ultrasound-Assisted Synthesis of a ZnO/BiVO4 S-Scheme Heterojunction Photocatalyst for Degradation of the Reactive Red 141 Dye and Oxytetracycline Antibiotic[J]. ACS Omega, 2023, 8(5):18.

[23] Preparation of Dual Z-scheme Bi2MoO6/ZnSnO3/ZnO Heterostructure Photocatalyst for Efficient Visible Light Degradation of Organic Pollutants[J]. Journal of Inorganic and Organometallic Polymers and Materials,2026,1-13.

[24] Guan G, Ye E, You M, et al. Hybridized 2D Nanomaterials Toward Highly Efficient Photocatalysis for Degrading Pollutants: Current Status and Future Perspectives[J]. Small (Weinheim an der Bergstrasse, Germany), 2020, 16(19)

[25] Chen H, Wei G, You Z, et al. Ca substitution improves the catalytic activity of perovskite LaCoO3 toward toluene: comprehension of electronic structure alteration[J]. Chemical Communications, 2023, 59(80):4.

[26] Chu L, Zhang J, et al. Solar-driven photocatalytic removal of organic pollutants over direct Z-scheme coral-branch shape Bi2O3/SnO2 composites[J]. Materials Characterization,2020,159.

[27] Wang B, Li X, Liang S, et al. Adsorption and oxidation of SO2 on the surface of TiO2 nanoparticles: the role of terminal hydroxyl and oxygen vacancy–Ti3+ states[J]. Physical Chemistry Chemical Physics, 2020, 22.

[28] Adriana M, Alberto J S, Victor Z, et al. Study of the Response Surface in the Photocatalytic Degradation of Acetaminophen Using TiO2[J]. Photochem,2022,2(1):225-236.

[29] Idriss H .On the wrong assignment of the XPS O1s signal at 531–532eV attributed to oxygen vacancies in photo- and electro-catalysts for water splitting and other materials applications[J].Surface Science, 2021, 712:121894.

[30] Ma H, Hao B, Song W, et al. A High-Efficiency TiO2/ZnO Nano-Film with Surface Oxygen Vacancies for Dye Degradation.[J]. Multidisciplinary Digital Publishing Institute, 2021(12).

[31] Xu L, Ma X, Sun N, et al. Bulk oxygen vacancies enriched TiO 2 and its enhanced visible photocatalytic performance[J]. Applied Surface Science,2018,441150-155.

[32] Zhen W, Wenchao W, Wen L, et al. Steering Electron–Hole Migration Pathways Using Oxygen Vacancies in Tungsten Oxides to Enhance Their Photocatalytic Oxygen Evolution Performance[J]. Angewandte Chemie International Edition,2021,60(15):8236-8242.

[33] Xing J, Liu Y, Mathew G, et al. High-Entropy Metal–Organic Frameworks and Their Derivatives: Advances in Design, Synthesis, and Applications for Catalysis and Energy Storage[J]. Advanced Science, 2025, 12(5).

[34] Liu X, Chao J, Guo F, et al. Gd and Zr Co-Doped BiFeO 3 Magnetic Nanoparticles for Piezo-Photocatalytic Degradation of Ofloxacin[J]. Nanomaterials, 2025, 15(11).

[35] Singh P, Pandey G, Murti Y, et al. Light-driven photocatalysis as an effective tool for degradation of antibiotics[J]. RSC Advances, 2024, 14(29):20492-20515.

[36] Shang Q, Liu X, Zhang M. Photocatalytic degradation of ofloxacin antibiotic wastewater using TS-1/C3N4 composite photocatalyst: Reaction performance optimisation and estimation of wastewater component synergistic effect by artificial neural network and genetic algorithm[J]. Chemical engineering journal, 2022,443.

[37] Zhang D, Qi J, Ji H, et al. Photocatalytic degradation of ofloxacin by perovskite-type NaNbO3 nanorods modified g-C3N4 heterojunction under simulated solar light: Theoretical calculation, ofloxacin degradation pathways and toxicity evolution[J]. Chemical Engineering Journal, 2020, 400(000).

[38] Olsavsky N J, Kearns V M, Beckman C P, et al. Research and Regulatory Advancements on Remediation and Degradation of Fluorinated Polymer Compounds[J]. Applied Sciences, 2020, 10(19):6921.

[39] Aryan, V.; Font-Brucart, M.; Maga, D. A comparative life cycle assessment of end-of-life treatment pathways for photovoltaic backsheets. Prog. Photovolt. Res. Appl. 2018, 26, 443–459.